

**Quantifying the Binding Affinity of  
Disease Linked Ras Mutants to the Ras  
Binding Domain of PI3K $\gamma$  by Microscale  
Thermophoresis**

**Corey D. Tesdahl**

**Department of Biochemistry**

Defense Date: April 12<sup>th</sup>, 2023

**Defense Committee**

Dr. Joseph Falke (BCHM) –Thesis Advisor

Dr. Jeffrey Cameron (BCHM)—Honors Council Representative

Dr. Alison Vigers (PSYC &NRSC)—Outside Reader

## Abstract

The Ras family of GTPases (H/K/N-Ras) mediate numerous signaling pathways involved in cell proliferation, metabolism and cell motility through effectors such as Raf and phosphatidylinositol-3-kinase (PI3K). Ras bound to GTP adopts an active conformation that is able to bind to its effectors. Its intrinsic GTP hydrolysis activity yields an inactive, GDP-bound conformation, regulating the activation of its effectors as a molecular “on-off” switch. Ras mutations are present in around 30% of human cancers, predominantly in positions 12, 13, and 61. Mutations at these positions are thought to inhibit downregulation by GTPase Activating Proteins (GAPs) that normally increase its intrinsic rate of GTP hydrolysis by several orders of magnitude, leaving Ras in a constitutively activated form that hyperactivates effector pathways. However, a significant number of disease-linked Ras mutations occur at other positions. Notably, over 30 occur at interfacial positions that contact the Ras Binding Domain (RBD) of PI3K. We hypothesize that some of these mutations may increase (or decrease) the binding affinity of Ras to PI3K, which in turn would be predicted to recruit more (or less) PI3K to the plasma membrane and increase (or decrease) production of the signaling lipid phosphatidylinositol-3,4,5-triphosphate (PIP<sub>3</sub>). An increase in PIP<sub>3</sub> production is observed in many human cancers and is thought to hyperactive downstream effectors of the PI3K/Akt/mTOR pathway involved in the regulation of cellular growth. A decrease in PIP<sub>3</sub> production, by contrast, may yield growth defects that underly other human diseases linked to growth deficiencies.

The work presented in this thesis builds off of the significant progress of previous lab members, who designed the protein constructs used in this project and the methods for purification. My work includes optimizing the existing protein purification methodology and improving the microscale thermophoresis (MST) assay used to quantify the binding affinity of

Ras to the RBD of PI3K $\gamma$  in solution. I also helped design a robust method to standardize the analysis MST data. Perhaps most significantly, I collected MST data extensively, in conjunction with my undergraduate colleague Ian Fleming, that characterize the binding affinity of standard Ras, GDP-loaded standard Ras, and the Ras variants Q25L, D38E, Y40C, and R41Q to the PI3K $\gamma$  RBD. Our initial work has been published in *Analytical Biochemistry* (2022), in a paper reporting the first Ras mutation, Q25L, found to trigger increased affinity for Ras binding to the PI3K $\gamma$  RBD. More recently, new findings first presented herein show that the Ras mutation R41Q triggers an even larger increase in Ras affinity for Ras binding to the PI3K $\gamma$  RBD. Future work by the single molecule subgroup in our laboratory will test our predictions that (i) the Ras Q25L and R41Q mutations will each generate increased binding of full length PI3K to membrane-anchored Ras on a target membrane, and (ii) the resulting larger population of active, membrane-bound PI3K lipid kinase molecules will in turn exhibit increased net PIP<sub>3</sub> production under physiological conditions.

# Introduction

**Significance of Ras in Cancer and Disease.** The Ras family of proteins (H/K/N-Ras) are GTPases that act as binary switches between “on” and “off” states to regulate a variety of signaling pathways, including the Ras/mitogen-activated protein kinase (MAPK) and PI3K/Akt/mTOR pathways (Figure 1) [1,2]. Activation of Ras is achieved by the binding of GTP to the GTPase domain of the protein, stabilizing the “on” state. This is mediated by inputs from cellular receptors such as tyrosine kinase receptors (RTKs) and G-protein couple receptors (GPCRs) [2]. Ras activation is stimulated by guanine nucleotide exchange factors (GEF), which facilitate the exchange of GDP-bound Ras to GTP-bound Ras [2]. Another class of proteins known as GTPase-activating proteins (GAPs) serve to inactivate GTP-bound Ras by increasing the GTPase’s intrinsic hydrolysis ~1000 times [3].

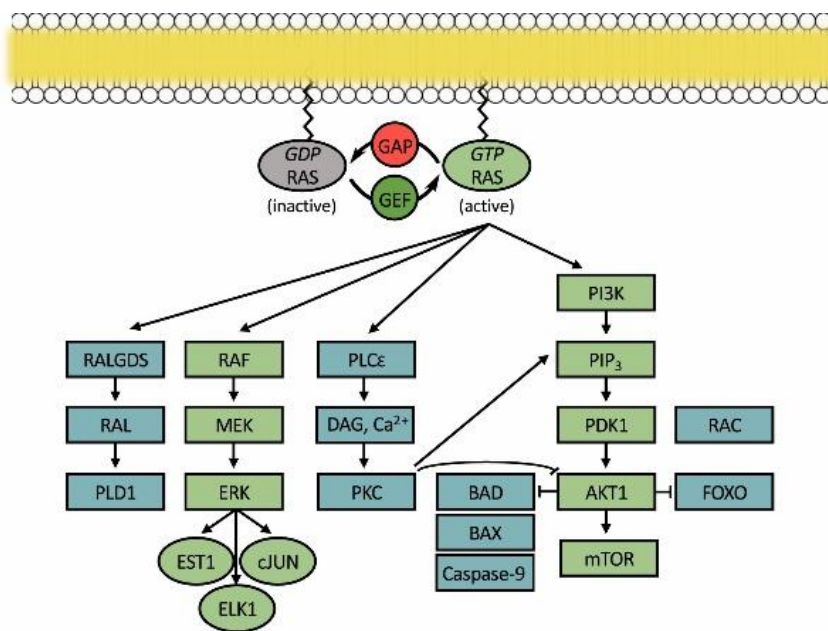


**Figure 1. Simplified schematic illustrating the cellular signaling pathways regulated by Ras.** From Fleming et al (2022) [4], modified from Lim et al (2019). Used with permission. Figure by Corey Tesdahl and Joseph Falke.

Ras signaling has been shown to affect cellular growth and survival, metabolism and cell motility. Its dysregulation is associated with a variety of cancers and developmental disorders [1]. Roughly 30% of all human tumors that are screened possess mutations to one of the three Ras genes. K-Ras is the most frequently mutated isoform (21%), followed by N-Ras (8%) and H-Ras (3%). [5,6,7]. These three Ras isoforms share 95% sequence identity throughout the first 164 residues that comprise the G domain involved in GTP binding and hydrolysis, and differ in the variable C-terminal region [8]. The vast majority of Ras mutations occur at residues 12, 13, and 61, which are thought to impair the GAP-mediated GTP hydrolysis that switches Ras to an off state [9].

In addition to the somatic Ras mutations observed in many cancers, germline mutations in *Ras* genes have been shown to cause disease. A collection of congenital Ras mutations are found in phenotypically similar developmental disorders. This group of closely related disorders, sometimes referred to as RASopathies, includes neurofibromatosis type 1 (NF1), Costello's syndrome (specific to H-Ras), and Noonan's syndrome. These disorders may trigger excessive growth or slowed growth (growth defects). Many of these disorders may also arise from germline mutations to genes besides Ras that code for other components and regulators of the Ras/MAPK pathway [10]. The best characterized disease-linked Ras mutations lie at the 12,13, and 61 hotspot positions located in or near the GTPase active site, where they inhibit intrinsic GTPase activity and/or the GTPase-stimulating interaction with GAPs. These mutations yield excessive Ras activation and upregulation of multiple Ras-regulated pathways. Many other Ras mutations are located distal to the active site and do not perturb GTPase activity, and thus likely trigger disease by alternative mechanisms [8]. Notably, the effect of Ras mutations on the regulation of the PI3K/Akt/mTOR pathway has not been systemically studied [11].

***Ras Plays an Essential Role in Maximal PI3K Activation.*** lipid kinase PI3K is another potent oncogene commonly mutated in human cancers [12]. PI3K generates the signaling lipid phosphatidylinositol-3,4,5-triphosphate (PIP<sub>3</sub>) via phosphorylation of phosphatidylinositol-4,5-biphosphate (PIP<sub>2</sub>). Aside from its global presence as a potent growth signal in normal cell growth, PIP<sub>3</sub> plays an essential role at the leading-edge plasma membrane of chemotaxing leukocytes [13]. Previous single-molecule, biophysical studies have demonstrated that the presence of membrane anchored Ras is necessary to achieve maximal PI3K activation, acting synergistically with an RTK-derived phospho--tyrosine polypeptide to activate PI3K (Figure 2,3A) [14]. The Ras-PI3K binding interaction recruits more PI3K to the membrane, increasing the amount of the membrane-anchored PI3K and a resulting proportional increase in PIP<sub>3</sub> production [4,14].

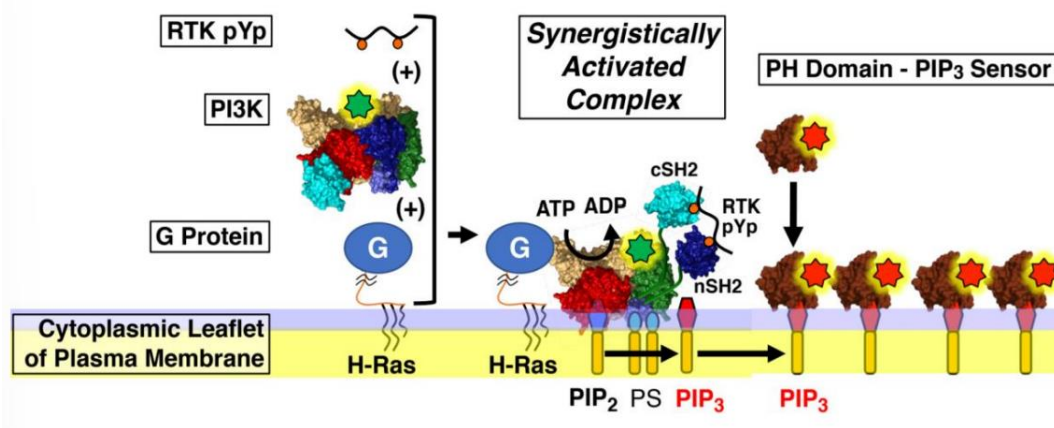


**Figure 2. Membrane-anchored Ras recruits PI3K to the plasma membrane, increasing PIP<sub>3</sub> production.** Ras and a phospho-tyrosine polypeptide (pYp) recruit PI3K to the plasma membrane and activate it. Activated PI3K phosphorylates PIP<sub>2</sub> to the signaling lipid PIP<sub>3</sub>. From Buckles et al (2017), used with permission. Figure by Tom Buckles and Joe Falke.

***Certain Ras Mutants May Perturb the Ras-PI3K Binding Interaction.*** There are over 30 Ras mutations located at the 10 perfectly conserved Ras positions that directly contact the Ras Binding Domain (RBD) of PI3K [6,15]. An important step in better understanding the biological effect of these disease-linked Ras mutants is to investigate whether these mutations significantly perturb the Ras-PI3K binding affinity, potentially dysregulating PIP<sub>3</sub> and downstream components of the PI3K/Akt/mTOR pathway. Our laboratory hypothesizes that (i) one set of Ras mutants may increase binding affinity to the RBD of PI3K, thereby hyperactivating the PI3K/Akt/mTOR signaling pathway and triggering excessive growth diseases such as cancer, that (ii) another set of Ras mutants may decrease binding affinity to the RBD of PI3K yielding decreased pathway activation and growth defects, while a (iii) third set of mutants may have little or no effect on the binding affinity of Ras to the RBD of PI3K.

A crystal structure of the Ras-PI3K $\gamma$  interface by Pacold et al (2000) highlights the 10 Ras residues contacting PI3K $\gamma$  Ras binding domain that are 100% conserved (identical) between the three isoforms (Figure 3B,C) [16]. Similarly, the entire G domain of Ras is 95% conserved between the three Ras family members [7]. Hence, the H-Ras, K-Ras and N-Ras isoforms share virtually identical binding sites for the docking of PI3K RBD. Notably, it follows that any disease-linked Ras mutation found at one of the 10 RBD contact positions in one Ras isoform is predicted to have the same effect on the binding of all three Ras isoforms to the RBD.

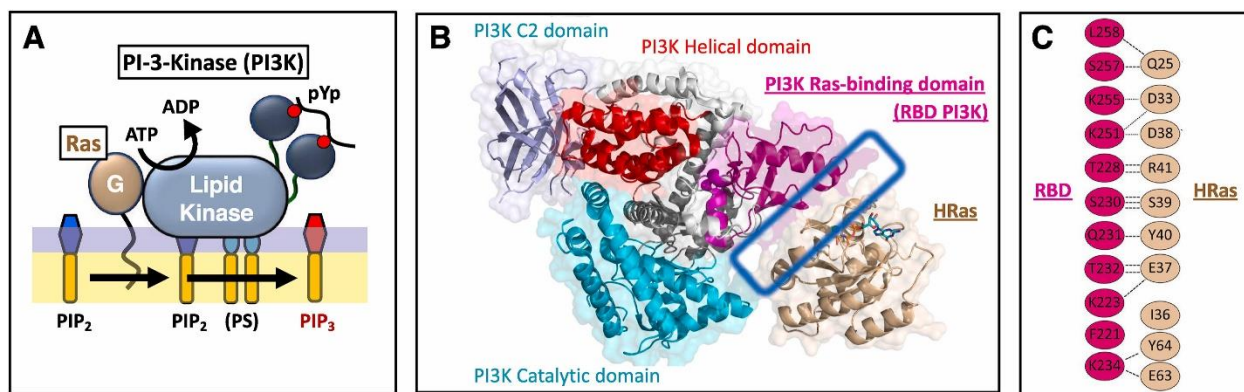


**Figure 3. The binding interface between Ras and PI3K.** (A) Ras recruits the lipid kinase PI3K to the plasma membrane. (B) Cartoon ribbon diagram of the binding interface between H-Ras and PI3K (Pacold et al, 2000) [16]. (C) H-Ras and PI3K residues contacting along the Ras-RBD interface with proposed salt bridges, represented by short dashes, and hydrogen bonds represented by long dashes. From Fleming et al (2022) [4], used with permission. Figure by Dr. Jonathan Hannon.

*Quantifying the Binding Affinity of Active H-Ras to PI3K $\gamma$ .* A novel, robust quantitative assay has been developed to investigate whether disease-linked Ras mutants perturb the binding affinity to PI3K $\gamma$ . The design of this assay and the initial protocols used to purify the H-Ras and PI3K $\gamma$  proteins constructs used in the assay were generated by former lab members Justin Martyr (CU Boulder Honors Thesis), Nick Cordaro (CU Boulder Honors Thesis), Dr. Hayden Swisher (CU Boulder PhD Thesis), and Dr. Jonathan Hannan. Further optimization of these protocols was carried out by me and my colleague, Ian Fleming as reported herein.

The standard H-Ras protein construct employed in this assay to approximate wild-type H-Ras has been well used and characterized in the field. Because the three Ras isoforms share high sequence homology through the entire G-domain, this standard H-Ras construct should be representative of the binding interaction of all three [7]. This standard H-Ras was modified by site-directed mutagenesis to generate a set of Ras point mutants that we investigated in the

standard H-Ras background [15]. The soluble PI3K $\gamma$  RBD construct used includes residues 220-311 (the RBD), fused between an N-terminal maltose-binding protein (MBP) and a C-terminal green fluorescent protein Clover. Previous quantification of wild-type Ras binding to full length PI3K $\gamma$  has reported near identical binding affinity, with a reported  $K_D$  within two-fold to what we have observed in our binding assays [16,17].

In order to establish a robust quantitative assay, two critical methods were used to accurately quantify the concentration of active Ras. A simple  $A_{280}$  UV-vis measurement is not sufficient to accurately determine its concentration because Ras is completed with guanine nucleotide, thus introducing significant absorption from the nucleotide at 280nm. A UV-deconvolution protocol developed by Dr. Hayden Swisher utilizes reference spectra for apo-Ras and guanine nucleotide to deconvolute the absorption of the protein component, a method that has been verified by amino acid analysis [18]. From this, the Beer-Lambert law can be used to determine the concentration of Ras. Another critical consideration is that only active Ras binds significantly to PI3K, where active Ras is defined as the population of Ras bound to GTP or a non-hydrolysable GTP analog. A method using HPLC, developed by Dr. Jonathan Hannan, was employed to quantify the proportion of Ras bound to either GTP or the non-hydrolysable analog GMPPNP, representing the total proportion of active Ras [19]. Further, this HPLC method accounts for differences in active nucleotide loading between protein purifications. These two well established methods were used to characterize the binding interaction between Ras and PI3K as robustly as possible.

Microscale thermophoresis (MST) was used to quantify the binding interaction between our H-Ras and PI3K $\gamma$  constructs. The MST instrument used generates a thermal gradient (6°C) while measuring the relative rate of net diffusion of a fluorescent marker. In the case of our

assay, this fluor was Clover complexed to the RBD PI3K $\gamma$  construct. The diffusion constant of the fluorescence complex is dependent on a variety of factors such as molecular mass, shape, charge, and hydration shell [20]. When the RBD construct binds to Ras, the diffusion constant of this protein-protein complex changes in a way that is proportional to the fractional occupancy of the RBD, and subsequently so does the relative net diffusion of the fluorescent marker (the MST signal) [20]. A titration series of increasing Ras concentration ranging from the completely unbound fluorescent RBD construct to the fully saturated fluorescent RBD construct allows robust analysis MST assays to generate  $K_D$  values of the Ras-RBD interaction for standard Ras and Ras variants (Figure 4). The concentration of the fluorescent RBD construct is kept constant through the titration.

Our findings indicate that all 4 H-Ras mutants examined in positions contacting the RBD of PI3K $\gamma$  show perturbed binding compared to standard Ras. One mutation distal to the Ras-PI3K $\gamma$  binding interface showed no significant change in binding affinity from standard Ras. Inactivated Ras, bound to GDP, showed a decrease in binding affinity by 1-2 orders of magnitude. Collectively, these findings demonstrate that certain H-Ras mutations do indeed perturb binding affinity to PI3K $\gamma$ , which may result in significant changes in activity of the PI3K/Akt/mTOR pathway.

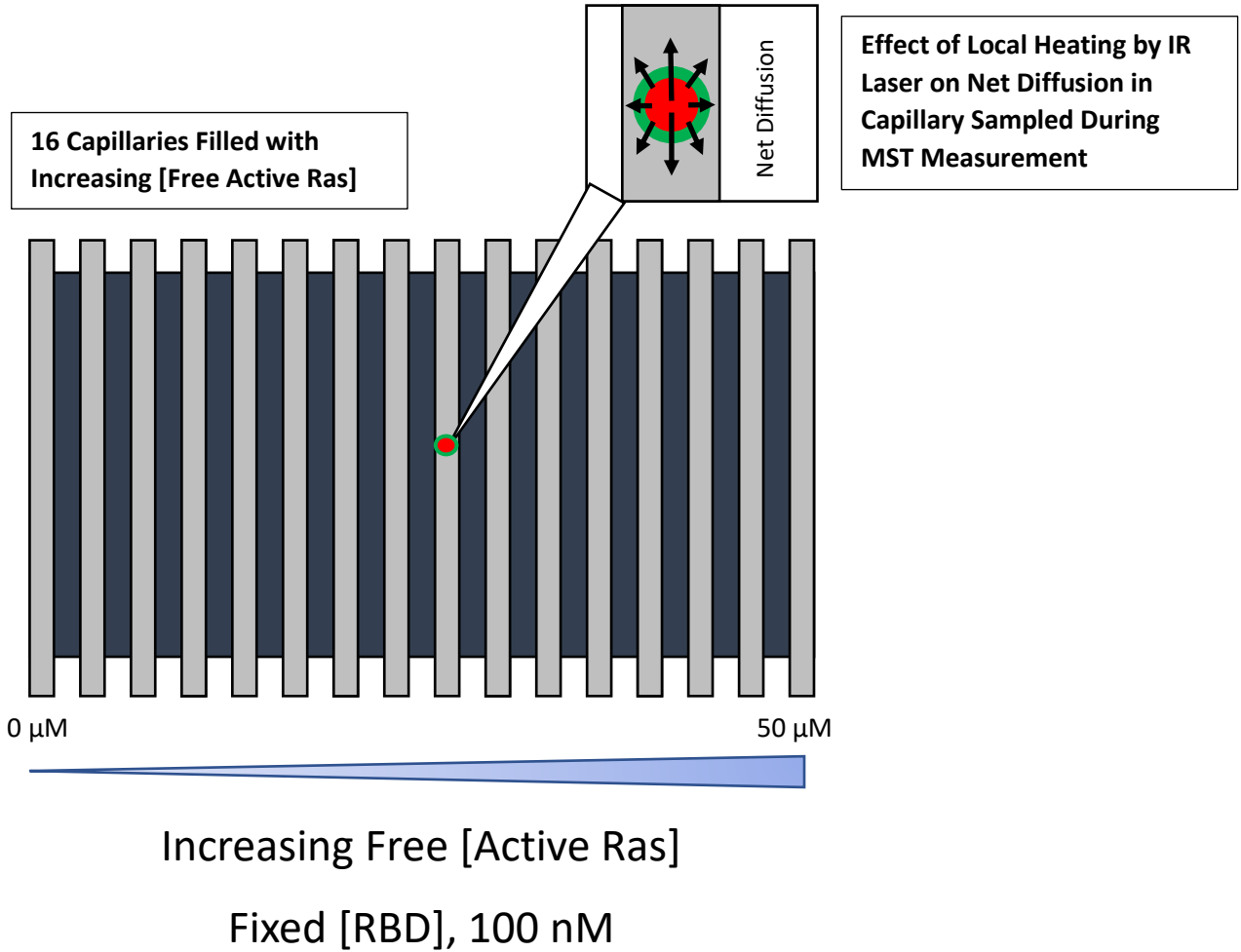


**Figure 4. Representation of the microscale thermophoresis binding assay.** Each capillary is filled with a solution consisting of Ras, in increasing concentration from left to right, and the fluorescent RBD, kept at a constant concentration throughout the titration. A blue light source is applied and the GFP component of the fluorescent RBD which fluoresces green light (represented by the circular green border). An IR laser (represented by the red circle) is briefly applied to generate a thermophoretic gradient. Net diffusion proceeds down the gradient as indicated by arrows, yielding the MST signal monitored by the instrument. Figure by Corey Tesdahl.

## Methods

The methods for this project outlined below are taken with minor modifications from the a previously published paper by the lab, on which I am a co-first author and personally wrote much of (Fleming et al, 2022) [4]. Used with permission.

**Reagents.** *E. coli* BL21 cells were obtained from New England Biolabs (Ipswich, MA), and Bacto yeast extract, agar and tryptone for bacterial growth were from Gibco (Waltham, MA). Ampicillin and HEPES free acid were from Research Products International (Mount Prospect, IL). Kanamycin and reduced L-glutathione were from Sigma-Aldrich (St. Louis, MO). Phenylmethylsulfonyl fluoride (PMSF) used to inhibit proteolysis during Ras purification was from Roche Diagnostics (Basel, Switzerland). TALON cobalt(II) metal affinity resin for polyhistidine tag purification was from Takara (Kusatsu Japan), and HYDRANAL imidazole was from Honeywell (Charlotte, NC). Ethylenediamine tetracetic acid disodium salt dihydrate (EDTA) was from Thermo Fisher Scientific (Waltham, MA). Non-hydrolyzable GTP analog GMPPNP, conjugated with four lithium counter ions, at >95% purity, was from Abcam (Cambridge, UK). Guanosine 5'-diphosphate [GDP] disodium salt was from Sigma-Aldrich (St. Louis, MO). Desalting columns were Econo-Pac 10DG desalting prepacked gravity flow columns from Bio-Rad (Hercules, CA). Vivaspin 500, 10,000 MWCO spin concentrators from Sartorius were used to concentrate protein samples (Göttingen, Germany). Microscale thermophoresis measurements were performed on a Nanotemper Monolith NT.115 instrument utilizing Monolith NT.115 capillaries (Munich, Germany).

**H-Ras Plasmid Construct and Mutagenesis.** An H-Ras expression plasmid was previously gifted by the Groves lab, comprising an N-terminal hexahistidine tag and the first 184 residues of the canonical H-Ras sequence, including the point mutation C118S and the C-

terminal deletion  $\Delta 185-189$ . A modified version of this construct, additionally containing a C181S substitution, was used in this study [14,18,19]. The resulting C118S/C181S H-Ras 1-184 construct retains a single Cys residue (C184) for follow-up studies of membrane-anchored H-Ras in the reconstituted Ras-PI3K-PIP<sub>3</sub> signaling pathway [14]. This construct, which approximates the ‘wild-type’ H-Ras sequence and retains all native contact residues for PI3K $\gamma$  Ras binding domain, is hereafter referred to as ‘standard’ H-Ras. The other H-Ras variants employed were created in the standard H-Ras background by introducing a single point mutation (G13R, Q25L, D38E, Y40C, or R41Q) using the QuikChange mutagenesis kit from Agilent Technologies (Santa Clara, CA) and mutagenesis DNA primers from Integrated DNA Technologies (Coralville, IA), followed by sequencing of the full H-Ras gene by GENEWIZ (South Plainfield, NJ). To isolate plasmid for sequencing and future protein expression, the mutagenesis reaction was transformed into DH5 $\alpha$  *Escherichia coli* cells and grown on 2xYT agar plates containing 50  $\mu\text{g}/\text{mL}$  ampicillin for 18 h at 37 °C. Single colonies were inoculated into culture flasks with 5 mL of 2xYT media and the same ampicillin concentration. Following 15 h of shaking incubation at 37 °C, the OMEGA Bio-Tek E.Z.N.A. Plasmid DNA Mini Kit (Kansas City, MO) was used to purify the H-Ras plasmid. The mutant gene sequence was confirmed using Sanger sequencing through GENEWIZ.

***Ras Protein Expression and Purification.*** H-Ras plasmids were transformed in BL21(DE3) chemically competent *E. coli* cells and grown on 2xYT + agar plates with 100  $\mu\text{g}/\text{mL}$  ampicillin for 16 h at 37 °C. Single colonies were inoculated into 12.5 mL of 2xYT media supplemented with 50  $\mu\text{g}/\text{mL}$  ampicillin and grown for 15 h at 37 °C, shaking at 250 rpm. This culture (12.5 ml) was diluted into 750 mL of media of the same composition and grown as above for approximately 2.5–3 h until an OD<sub>600</sub> reading of 0.4 was reached. Protein expression

was induced by addition of isopropyl  $\beta$ -D-1-thiogalactopyranoside (IPTG) (Invitrogen, Waltham MA) to 500  $\mu$ M then the cultures were incubated with shaking at 18 °C for 18 h. Cells were pelleted by centrifugation at 4000 $\times$ g for 15 min at 4 °C and then resuspended to 35 mL total volume in ice cold Lysis Buffer (50 mM Na<sub>2</sub>HPO<sub>4</sub>, 150 mM NaCl, 1 mM MgCl<sub>2</sub>, 2.5 mM glutathione, 1 mM PMSF, pH 8.0). Cells were lysed by sonication and cellular debris were removed by centrifugation at 30,000 $\times$ g for 25 min at 4 °C. The clarified supernatant was passed through a 20 mL Bio-Rad Econo-Pac® chromatography column (Hercules, CA) containing 1.5 mL Talon cobalt(II) resin and the 6X N-terminal His-tagged Ras protein bound to the resin was successively washed with 9 mL of ice cold Wash 1 buffer (50 mM HEPES, 150 mM NaCl, 1 mM MgCl<sub>2</sub>, 2.5 mM glutathione (fresh), 1 mM PMSF, pH 8.0) and 6 mL of ice cold Wash 2 Buffer (Wash 1 Buffer + 10 mM imidazole), then eluted with 4 mL of Elution Buffer (50 mM HEPES, 300 mM NaCl, 1 mM MgCl<sub>2</sub>, 250 mM imidazole, 2.5 mM glutathione, pH 8.0) all in a cold room at 4 °C.

***PI3K $\gamma$  RBD Construct: Purification, Characterization and Storage.*** The PI3K $\gamma$  Ras Binding Domain (RBD) plasmid construct was created from the pET MBP mClover LIC cloning vector plasmid (Addgene, Watertown, MA) containing an N-terminal 6x His tag, maltose binding protein (MBP) to stabilize isolated domain inserts, and the green fluorescent protein (GFP) Clover. The MBP and GFP were separated by an unstructured linker including a predesigned ligation independent cloning (LIC) site for direct insertion of residues 220-311 of PI3K $\gamma$  RBD.

A protocol similar to that described above for H-Ras expression and purification was utilized to isolate the RBD construct. The MBP-RBD-GFP plasmid was transformed into *E. coli* as described above, then plated on 50  $\mu$ g/mL kanamycin 2xYT agar plates. A single colony

was used to inoculate 50 mL of 2xYT media containing 50 µg/mL kanamycin. Following 2 h of incubation at 37 °C with shaking at 250 rpm, 50 µM IPTG was added to induce protein expression followed by 20 h of incubation at 30 °C with shaking at 250 rpm. Cells were pelleted by centrifugation at 4000×g at 4 °C and resuspended to 35 mL total volume in Lysis Buffer (see above). This resuspension was sonicated, and cellular debris was removed by centrifugation at 14,000×g at 4 °C. The supernatant was passed through 1.5 mL Talon cobalt(II) resin to bind to the His tag, and the bound protein was successively washed with 9 mL of ice cold Wash 1 and 6 mL of ice cold Wash 2 Buffer then eluted with 3 mL of Elution Buffer. Glycerol was added to eluent to a final concentration of 10%. The eluent was added to a 20 kDa MWCO dialysis cassette and was placed in Storage Buffer (25 mM HEPES, 140 mM KCl, 15 mM NaCl, 10% glycerol, 1 mM MgCl<sub>2</sub>, 2.5 mM glutathione, pH 7.4) for 4 h. The cassette was run through a second iteration of dialysis for 8 h. The concentration of the MBP-RBD-GFP protein in each sample was determined by measuring GFP absorbance at 505 nm on a NanoDrop One spectrophotometer (ThermoFisher), followed by application of Beer's Law and the known  $\epsilon_{505}$  of Clover GFP ( $\epsilon_{505} = 111,000 \text{ M}^{-1}\text{cm}^{-1}$  [21]). Finally, the purified protein was adjusted with Storage Buffer to ~25 µM final concentration, then snap frozen in 30 µL aliquots in liquid N<sub>2</sub> and stored at -80 °C.

***Ras Nucleotide Loading, Protein Concentration, and Storage.*** Eluted protein samples were further purified and transferred into Exchange Buffer (earlier protocol: 25 mM HEPES, 140 mM KCl, 15 mM NaCl, 1 mM MgCl<sub>2</sub>, 2.5 mM glutathione, pH 7.4; new protocol: same as previous protocol without 1 mM MgCl<sub>2</sub>) using Bio-Rad desalting columns at 4 °C. Subsequently, PhosSTOP (Sigma-Aldrich, Waltham, MA), a blend of phosphatase inhibitors, was added to the concentration recommended by the manufacturer and incubated at 37 °C for 20 min to eliminate

phosphatase activity. Exchange of endogenous nucleotide bound to Ras for a desired loading nucleotide was carried out at 37 °C by the following modification of a published protocol [22]. First, Ras-bound  $Mg^{2+}$  was chelated via addition of 10X EDTA stock buffer (100 mM EDTA in 25 mM HEPES, 140 mM KCl, 15 mM NaCl, pH 7.9) at 1:10 dilution to yield 10 mM EDTA final. Then, nucleotide exchange was triggered by addition of either activating GMPPNP nucleotide (a non-hydrolysable analogue of GTP) or inactivating GDP nucleotide from a 200 mM stock in exchange buffer to bring the exogenous nucleotide concentration to 15x the concentration of Ras. The ~1:10 mol ratio of  $Mg^{2+}$  to EDTA employed during the nucleotide exchange reaction yielded significant  $Mg^{2+}$  chelation, enabling adequate removal of bound  $Mg^{2+}$  from H-Ras to speed its nucleotide exchange, while minimizing the protein destabilization that could result from more extreme levels of  $Mg^{2+}$  chelation. Following the 20 min exchange reaction at 37 °C, excess  $Mg^{2+}$  was added via 1:10 dilution of 10X  $Mg^{2+}$  buffer (110 mM  $MgCl_2$ , 250 mM HEPES, 140 mM KCl, 15 mM NaCl, pH 8.0) to restore Ras to its native  $Mg^{2+}$ -bound state with very slow rates of nucleotide dissociation and exchange. The resulting sample was run through a Bio-Rad desalting column to remove unbound nucleotide while exchanging the protein-nucleotide complex into final Storage Buffer (25 mM HEPES, 140 mM KCl, 15 mM NaCl, 10% glycerol, 100  $\mu$ M EDTA, 1 mM  $MgCl_2$  2.5 mM glutathione, pH 7.4).

After exchanging the sample of Ras-nucleotide complex into Storage Buffer its Ras protein concentration was determined as follows. Each sample possessed significant absorption at 280 nm arising both from protein and nucleotide components, thus a UV deconvolution protocol was used to determine the protein component of the total  $A_{280}$  for determination of the protein concentration. This UV deconvolution method has been previously validated and described in detail [18]. Briefly, the 250-300 nm UV spectrum for each Ras sample was

measured on a NanoDrop One spectrophotometer (Thermofisher), then deconvoluted into its separate protein and nucleotide spectral components using predetermined apo-Ras and guanine nucleotide reference spectra and a standard spectral deconvolution software package (A|E – UV–Vis IR Spectral software (A|E, Version 2.2; [www.fluortools.com](http://www.fluortools.com)). Subsequently the Ras protein concentration was calculated from the protein component of  $A_{280}$  via Beer's Law and the apo-Ras  $\epsilon_{280}$  of  $19,370 \text{ M}^{-1}\text{cm}^{-1}$  (predicted from its primary sequence using ExPASy ProtParam [23]). This UV deconvolution procedure was highly reproducible: triplicate aliquots of the same sample were routinely analyzed by measuring and deconvoluting their 250–300 nm UV spectra, and the resulting triplicate measurements of protein concentration routinely varied less than 1%. Our previous studies also validated the accuracy of the UV deconvolution method by comparing the protein concentrations obtained for aliquots of the same sample by independent UV deconvolution and amino acid analysis, which agreed within  $1.7 \pm 1.6\%$  [18].

Following analysis of each sample to determine the Ras protein concentration, the sample was concentrated to  $\sim 200 \mu\text{M}$  using Vivaspin 500, 10,000 MWCO spin concentrators (Sartorius, Göttingen, Germany) [18]. Finally, a high-speed centrifugation step was performed at  $372,000\times g$  for 20 min at  $4 \text{ }^\circ\text{C}$  to pellet aggregates before snap freezing  $50 \mu\text{L}$  aliquots of supernatant in liquid nitrogen, followed by storage at  $-80 \text{ }^\circ\text{C}$ .

***SDS-PAGE Analysis of Protein Purity.*** After isolating Ras proteins, SDS-PAGE gels were employed to evaluate protein purity. A standard Laemmli buffer system was incorporated into a 9.5% stacking gel and a 12.5% separating gel, both 39:1 acrylamide:bisacrylamide. Samples stored at  $-80 \text{ }^\circ\text{C}$  (see above) were prepared by thawing on ice, diluting 1:10 dilution with storage buffer, then diluting 1:2 with 2X Loading Buffer (0.125 M Tris, 4.1% (w/v) SDS, 30% glycerol, 0.025% bromophenol blue, 40 mM DTT, pH 6.8). Samples were immediately

heated for 1.0 min at 95 °C then loaded onto the gel and run at a constant voltage of 125 V for 45 min, stained with Coomassie brilliant blue, and destained. Gel images were captured by a LAS 4000 Imager (ImageQuant, Sunnyvale, CA).

***Microscale Thermophoresis Measurements of Ras-RBD Binding.*** The Ras-RBD MST binding assay was carried out as follows to determine the equilibrium dissociation constant ( $K_D$ ) for the binding of each H-Ras protein to the isolated RBD in solution. First, Ras protein aliquots were thawed on ice and Vivaspin 500 centrifugal concentrators were rinsed with 500  $\mu$ L of Ligand Buffer (25 mM HEPES, 140 mM KCl, 15 mM NaCl, 1 mM  $Mg^{2+}$ , 2.5 mM glutathione, 10% glycerol, pH 7.4) by centrifugation at  $4500\times g$  for 3 min. Subsequently, 100  $\mu$ l of Ras was mixed with 500  $\mu$ L Ligand Buffer in each concentrator, then spun at  $4500\times g$  for 5 min thereby returning the Ras volume back down to 100  $\mu$ l. This step was repeated four more times for a total  $(1/5)^5 = 3000$ -fold wash of the protein with ligand buffer. A high-speed centrifugation step was performed at  $80,000\times g$  for 10 min to remove aggregates. The UV deconvolution protocol was performed as previously described [15] to find the concentration of total Ras protein. This concentration of total Ras was converted to the concentration of active Ras by multiplying with the fraction of active Ras, as determined by above HPLC quantification. The concentration of active Ras was adjusted to 100  $\mu$ M for the working Ras titration stock. The RBD construct MBP-RBD-GFP was thawed on ice and adjusted to a concentration of 200 nM for the working 2X RBD stock by dilution with Target Buffer (25 mM HEPES, 140 mM KCl, 15 mM NaCl, 1 mM  $Mg^{2+}$ , 2.5 mM glutathione, 1 mg/mL BSA, 1% Tween 20).

Each MST titration series was generated and subjected to MST analysis as follows. Sixteen Ras dilutions were carried out to create a set of 2X Ras stocks, then each was mixed 1:1 with the 2X RBD stock in three triplicate samples. The resulting three sets of 16 samples

possessed the same, fixed RBD concentration (100  $\mu\text{M}$ ) and varying active Ras concentrations (50  $\mu\text{M}$ , 50  $\mu\text{M}$ , 40  $\mu\text{M}$ , 35  $\mu\text{M}$ , 30  $\mu\text{M}$ , 25  $\mu\text{M}$ , 20  $\mu\text{M}$ , 16  $\mu\text{M}$ , 12  $\mu\text{M}$ , 8  $\mu\text{M}$ , 4  $\mu\text{M}$ , 2  $\mu\text{M}$ , 1  $\mu\text{M}$ , 0.5  $\mu\text{M}$ , 0  $\mu\text{M}$ , 0  $\mu\text{M}$ ). Approximately 7.5  $\mu\text{L}$  of each sample was loaded into an MST capillary for measurement, yielding three triplicate titration series. Each titration was then measured separately in the Nanotemper Monolith NT.115 instrument controlled by MO.Control software. Settings included blue excitation light source at 10% intensity, high IR laser power (yielding a 6  $^{\circ}\text{C}$  temperature increase above ambient at the center of the thermal gradient), sample chamber controlled at 22  $^{\circ}\text{C}$ , and capture of the MST signal 1.5 s after activation of the IR laser. Raw data, including the MST signal measured for each sample in a given titration, was exported using MO.Analysis software.

MST titration data was analyzed as follows. The MST signals obtained for the two negative control (0  $\mu\text{M}$  Ras) samples in the same titration were averaged and the resulting baseline value was subtracted from the MST signals of all sixteen samples of that titration, yielding their change in value from the average “zero-point”. The resulting three baseline-corrected triplicate titrations were averaged to generate a mean active Ras titration. To account for any underlying trend in the capillary positions (and time sequence) of the MST titration, “blank” runs (6 triplicate titrations) were performed in which the RBD construct was titrated with protein-free ligand buffer, then the 18 blank runs were baseline corrected and averaged to give the average blank titration. The resulting average blank titration was subtracted from the mean Ras titration to yield the buffer-corrected, mean active Ras titration.

Initial characterization of standard H-Ras and its mutants Q25L, D33E, and Y40C revealed that the Q25L Ras mutant possessed the highest RBD affinity and consistently reached maximal saturation during the Ras-RBD titration. This Q25L Ras was therefore chosen to serve

as the internal standard titration in all MST measurements. For each day of MST titrations, a triplicate Q25L titration was included both to monitor the experiment for inconsistencies and to quantify the maximal MST binding signal ( $B_{max}$ ) for the day. Once the buffer-corrected, mean Q25L active Ras titration was obtained, Prism software (GraphPad, San Diego, CA) was used to best-fit the binding equation  $Y = (B_{max} * X)/(X + K_D)$ , where  $X$  is the active Ras concentration, by nonlinear regression. The resulting best-fit Q25L  $B_{max}$  parameter represented the MST signal at full RBD saturation with bound Ras, and was found to be the same, within error, for Q25L and other high affinity proteins on the same measurement day. Next, for all mean active Ras titrations measured on the same day, each mean data point was divided by the best-fit Q25L  $B_{max}$  value, thereby converting each data point in the titration to a fractional RBD occupancy. Finally, the mean active Ras titration for each Ras protein was plotted as fractional RBD occupancy against active Ras concentration (Figure 8,9), and the best fit  $K_D$  value was determined by best fit of the binding equation  $Y = [X]/([X] + K_D)$ , where  $X$  is the active Ras concentration, via nonlinear regression.

After our publication comparing the RBD binding affinities of standard H-Ras and its mutants Q25L, D33E, and Y40C subsequent studies in collaboration with Ian Fleming revealed a new H-Ras mutant R41Q that possesses the highest RBD affinity observed thus far. It also possesses a maximum MST signal of ~20% greater magnitude than standard H-Ras and the other mutants studied to date, suggesting that the R41Q mutant alters the diffusion constant of the Ras-RBD complex compared to other H-Ras proteins. The MST signal is known to be sensitive to multiple components that impact the net diffusion constant of the bound complex, including its total mass, volume, shape, surface electrostatics, and associated solvation/ionic cloud. Evidently the R41Q surface charge mutation has a unique effect on one or more of these parameters, for

unknown reasons. As a result, for R41Q it was necessary to determine the best fit  $K_D$  value utilizing the binding equation  $Y = A*[X]/([X] + K_D)$ , where A is the floating variable defining the maximum value that the R41Q best fit asymptotically approaches.

**Statistics.** To ensure the rigor and reproducibility of  $K_D$  measurements, for each Ras protein at least 6 triplicate titrations were carried out on at least 6 different days. Moreover, the measurements for a given Ras protein employed at 2 separate protein preps, each used for at least 2 triplicate titrations. The resulting 6 + mean triplicate  $K_D$  values were averaged to yield a global average  $K_D \pm SEM$ , where the standard error of the mean was calculated for the total number ( $N \geq 6$ ) of triplicates. Finally, statistical analyses were carried out using a one-tailed T-test to calculate p values to determine whether the  $K_D$  value measured for standard H-Ras was significantly higher than variants showing weaker binding curves (D38E, Y40C, and GDP-Ras) or significantly lower than the variant showing tighter binding curves (Q25L). A two-tailed T-test was performed to determine if G13R had a significantly different  $K_D$  from standard H-Ras. T-tests were carried out using Excel (Microsoft, Seattle with unequal variances function) where  $p < 0.05$  (or  $< 5\%$  uncertainty) was required for significance.

## Results

***Soluble, Stable H-Ras and PI3K $\gamma$  Constructs Employed in These Studies.*** To measure the binding affinity of the Ras-PI3K $\gamma$  binding interaction by microscale thermophoresis, bacterial plasmids designed to express soluble protein constructs of each protein were created (Figure 5). The standard H-Ras construct employed includes modifications of wildtype H-Ras to facilitate purification and homogeneous membrane anchoring needed for future single molecule studies of the most interesting H-Ras mutants). A hexahistidine tag was included on the N-terminus to allow for protein purification by His-tag affinity chromatography. C118S and C181S mutations were introduced, and the 5 C-terminal residues were deleted, to leave a single, exposed native cysteine residue at the standard H-Ras C-terminus, C184, for future membrane anchoring [14]. The RBD construct consisted of residues 220-311 of the PI3K $\gamma$  p110 subunit, fused with an N-terminal maltose binding protein (MBP) and a C-terminal GFP Clover. This construct also contains an N-terminal hexahistidine tag for purification by affinity chromatography.

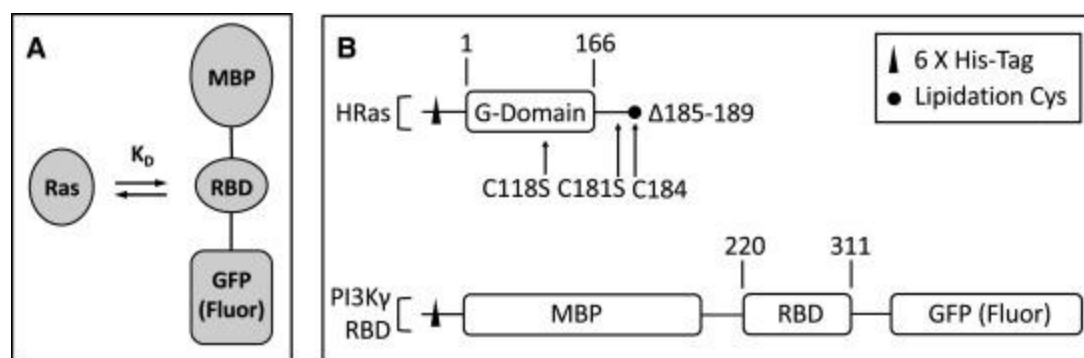


**Figure 5. Schematic illustrating the binding interaction between the soluble Ras and PI3K $\gamma$  constructs.** (A) The binding interaction of soluble Ras and PI3K constructs. (B) Representation of the modifications made to the Standard Ras construct from wild-type H-Ras, along with the components comprising the RBD PI3K $\gamma$  construct. From Fleming et al (2022), used with permission. Constructs created by Tom Buckles (H-Ras), and by Hayden Swisher and Nick Cordaro (RBD). Figure by Johnny Hannan and Joe Falke.

*Quantifying the Proportion of the Ras Population in the Active State.* Purification of Ras, loaded with the activating nucleotide GMPPNP by a nucleotide exchange step, was used to generate proteins stocks used in the microscale thermophoresis binding assays (Figure 6). A UV deconvolution step separated the apo-Ras and nucleotide spectral components contributing to the overall absorption spectrum, based on an established protocol [18]. The absorbance of the apo-Ras component, in combination with the extinction coefficient of Ras at 280nm ( $19,370 \text{ cm}^{-1}$ ), was used to determine the concentration of total Ras. Another step using an established HPLC protocol was used to quantify the proportion of activated Ras [19]. The proportion of active Ras for a given protein purification was found by HPLC analysis to range from 49% to 89% of the total Ras population in different Ras preps. This broad range is a result of the gentle nucleotide exchange process used to load Ras with GMPPNP while minimizing Ras perturbation, which yields variable GMPPNP loading. The broad range also emphasizes the importance of measuring the proportion of active Ras produced by nucleotide exchange, which is an important aspect of rigorous Ras prep analysis introduced by our laboratory. The active Ras subpopulation is the sum of the GTP and GMPPNP subpopulations present in analysis by HPLC. The bulk of the remaining Ras population is loaded with GDP and thus not active. Accounting for the proportion of active Ras in each purification standardizes analysis by microscale thermophoresis by enabling titrations with known concentrations of active Ras for every protein prep. HPLC analysis was carried out by Dr. Jonathan Hannon and Shea O'Conner (see Supplemental Table S1).

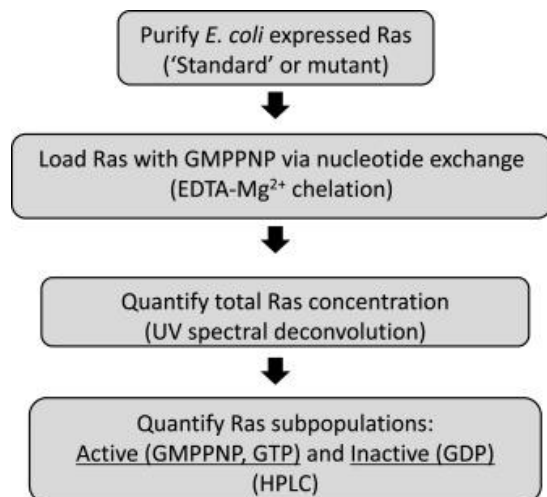


**Figure 6. Workflow to determine the concentration of active Ras used in microscale thermophoresis binding assays.** The quantification of active Ras determined by this method is used to generate a titration series with increasing active Ras for the microscale thermophoresis binding assay. All Ras preps carried out by Corey Tesdahl and Ian Fleming. HPLC analysis carried out by Johnny Hannan and Shea O'Connor. Figure by Johnny Hannan and Joe Falke.

*Microscale Thermophoresis Quantifies the Binding Affinity of Ras to PI3K $\gamma$ .* A binding assay for microscale thermophoresis was designed using the soluble Ras and PI3K $\gamma$  constructs. The concentration of the RBD construct was fixed to 100 nM throughout the MST titration and was determined by using the extinction coefficient of Clover at 505 nm ( $111,000 \text{ cm}^{-1}$ ), its absorbance at 505 nm ( $A_{505}$ ), and Beer's law. In each MST assay, two negative control titrations with the RBD construct and no Ras were included to establish the MST signal of the unbound RBD construct. An increasing concentration of Ras was titrated, beginning with 0.5  $\mu\text{M}$  and increasing up to 50  $\mu\text{M}$ . A plot of the resulting MST signal from each concentration of active Ras yields a binding curve that is well-fit by a square hyperbolic shape, indicative of saturating binding to a single type of independent binding sites (i.e., one binding site per RBD) (Figure 7). This fit is consistent with an MST signal, and an average macroscopic diffusion coefficient, that is linearly related to the fractional occupancy of the RBD with active Ras, a characteristic typically seen in MST experiments [20].

## Fractional Occupancy of Ras Binding Domain (RBD) of PI3K Bound to Activated H-Ras

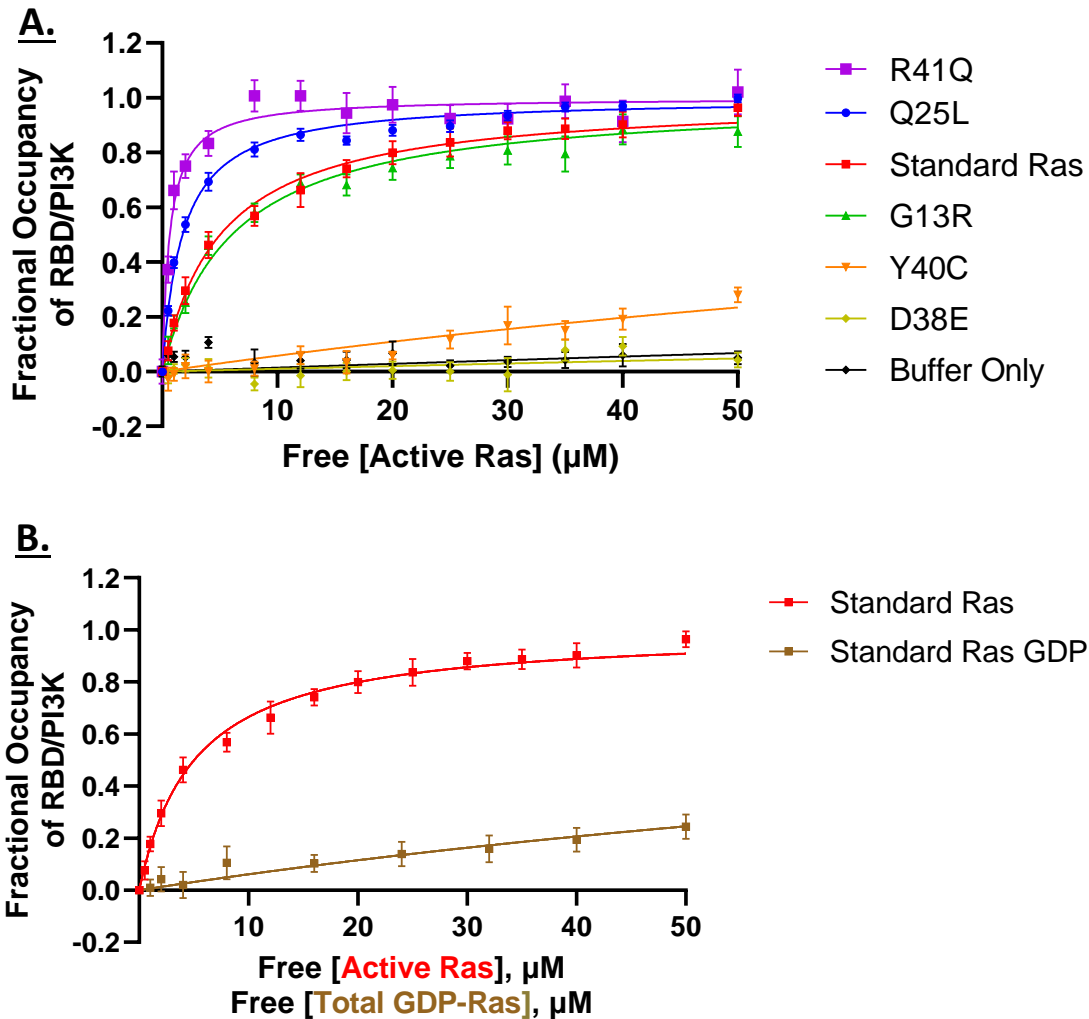


**Figure 7. Microscale thermophoresis quantifies the result of Ras mutations on binding affinity to RBD.** (A) Standard Ras or selected Ras mutants were loaded with activating nucleotide (GMPPNP or GTP). Ras was titrated into a fixed concentration of RBD (100 nM) and the MST signal at each concentration was recorded to plot the fractional occupancy of RBD against the concentration of free, active Ras. This plot was created by using the best fit of the standard binding equation for one independent binding site,  $F = [\text{Ras}]/([\text{Ras}] + K_D)$ . This yields the best-fit curves in this figure, as well as the dissociation constants for each Ras protein (Table 1). The only Ras variant not fit to this best-fit equation was R41Q, which instead used the equation  $F = A*[\text{Ras}]/([\text{Ras}] + K_D)$  where A is a floating variable reflecting its larger maximal MST signal. The R41Q data was then divided by A to normalize its maximal occupancy to 1.0 (see Methods for further details). (B) Standard Ras loaded with activating nucleotide compared to GDP-loaded Standard Ras. Because GDP-bound Ras does not bind with significant affinity to RBD, the concentration of free total GDP-Ras was used instead of free active Ras. Nonlinear

least squares best fit curves (solid lines) were determined by fitting the standard binding equation to the indicated average data points, yielding the following R-squared values: R41Q (0.940) Q25L (0.993), Standard Ras (0.994), G13R (0.990), Y40C (0.896), D38E (0.318), GDP-Standard Ras (0.930). Data and analysis by Corey Tesdahl and Ian Fleming.

The  $K_D \pm \text{SEM}$  ( $\mu\text{M}$ ) for standard Ras was determined to be  $6 \pm 1 \mu\text{M}$  (Table 1). This is within two-fold of previously reported  $K_D$  for full length PI3K $\gamma$  under similar physiological conditions [16]. Furthermore, the control mutations D33E and Y40C both showed significantly lower binding affinity than Standard Ras, with  $K_{DS}$  of  $600 \pm 100 \mu\text{M}$  and  $200 \pm 40 \mu\text{M}$ , corroborating previous qualitative studies of these two Ras mutants [16]. It is not possible to achieve saturating concentration with the inactive, GDP-loaded Ras, so an assumption was made that active and inactive Ras will reach the same maximum MST signal when the RBD is fully saturated with Ras. This is supported by a similarly strong fit for GDP-loaded Ras as the other Ras proteins. The  $K_D$  of GDP-loaded Ras  $260 \pm 90 \mu\text{M}$ , around 40 times lower than the  $K_D$  determined for standard Ras. These findings suggest nucleotide-dependent “on-off” switching that would be expected for native Ras binding to its effectors.

Notably, two mutations demonstrated significantly stronger binding affinity to the RBD of PI3K $\gamma$ . The mutant Q25L showed a three-fold increase in binding affinity compared to standard Ras, and the mutant R41Q showed a six-fold increase in binding affinity (Table 1). These mutants are at contact positions to the RBD of PI3K $\gamma$  and both have been found in one or more tumors. G13R, a cancer-linked hotspot mutation distal to the Ras-RBD interface was found to have a  $K_D$  of  $7 \pm 1 \mu\text{M}$ , which did not differ significantly from standard Ras. This mutant is known to inhibit the GTPase activity of Ras and thus, as expected, retained more bound GTP than the other mutants after GMPPNP loading (Table S1).

To ensure the accuracy and reproducibility of this approach to quantifying binding affinity, extensive average of replicates was performed. Each replicate (N) was an average of three triplicate MST measurements. At least 6 replicates were collected for each Ras protein consisting of at least 2 replicates from separate protein purifications. In order to standardize the analysis of Ras mutants, especially the Ras mutants that do not significantly approach saturation, the maximum MST signal for Q25L was used to determine the maximum MST signal other Ras mutants would have at saturation of the RBD. The mutant was chosen for this purpose because it is the highest-affinity Ras protein investigated that does not affect the diffusion coefficient of the saturated Ras-RBD complex.

**Table 1.**

| <b>Protein</b>          | <b><math>K_D \pm SEM</math> (<math>\mu</math>M)</b> | <b>Significance (p-value)</b> | <b>N (triplicates)</b> |
|-------------------------|---|-------------------------------|------------------------|
| <b>Standard Ras</b>     | $6 \pm 1$   | 1                             | 7                      |
| <b>G13R</b>             | $7 \pm 1$   | 0.4                           | 8                      |
| <b>Q25L</b>             | $2.0 \pm 0.2$                                       | 0.004                         | 22                     |
| <b>D38E</b>             | $600 \pm 100$                                       | 0.0009                        | 6                      |
| <b>Y40C</b>             | $200 \pm 40$  | 0.0009                        | 7                      |
| <b>R41Q</b>             | $1.1 \pm 0.5$                                       | 0.0013                        | 6                      |
| <b>Standard Ras GDP</b> | $260 \pm 90$  | 0.02                          | 6                      |

**Table 1.** Binding affinity ( $K_D$ ) of active H-Ras and H-Ras mutants to the Ras binding domain (RBD) of PI3K $\gamma$  in solution. A two-tailed t-test was used to evaluate significance of each protein compared to Standard Ras. Each triplicate (N) consists of three replicates. For example, analysis of Standard Ras included 7 triplicates and hence 21 individual replicates. Data and analysis by Corey Tesdahl and Ian Fleming.

## Discussion

**Assumptions.** Several implicit assumptions were made in the design of this project. An assumption was made that bacterially expressed soluble H-Ras and RBD constructs expressed in will approximate the binding of native H-Ras to full length native PI3K $\gamma$ . Evidence supporting the validity of this assumption is provided by the observation that the best fit  $K_D$  we observed for binding of the standard H-Ras construct to RBD ( $6 \pm 1 \mu\text{M}$ ) is within two-fold of a previously reported  $K_D$  of H-Ras to full length PI3K $\gamma$  ( $3.2 \pm 0.5 \mu\text{M}$ ) [16]. Another assumption is that the binding interactions between the present Ras and RBD constructs in solution will mimic the relative affinities observed between Ras constructs and full length PI3K on a target membrane surface. Native Ras is anchored to the plasma membrane by farnesylation of the C-terminal C181 or C184 residues when it recruits full length PI3K in the native binding reaction [24]. Both assumptions will be tested by future studies of membrane-anchored H-Ras binding to full length PI3K on a target membrane surface by our laboratory's single molecule TIRFM experiments that quantify this binding interaction and its effect on PI3K kinase activity and production of PIP<sub>3</sub> lipid.

***Two Previously Uncharacterized Disease-Linked Ras Mutations Demonstrate Increased Binding Affinity to the RBD of PI3K $\gamma$ .*** This study reveals that two cancer-linked Ras mutations demonstrate increased binding affinity to the RBD of PI3K $\gamma$  relative to Standard H-Ras, which exhibits a  $K_D$  of  $6 \pm 1 \mu\text{M}$ . The  $K_D$  of the R41Q variant was found to be nearly 6-fold lower at  $1.1 \pm 0.5 \mu\text{M}$ , with a significance of  $p = 0.0013$  compared to standard Ras. The  $K_D$  of the Q25L variant was found to be 3-fold lower at  $2.0 \pm 0.2 \mu\text{M}$  with a significance of  $p = 0.004$  compared to standard Ras. Interestingly, the R41Q variant showed a greater maximum MST signal than standard Ras or any other mutant. This indicates that H-Ras R41Q binding alters the

diffusion coefficient of the Ras-RBD complex by a larger magnitude compared to standard Ras and other variants. This could occur for a variety of reasons since the diffusion constant is sensitive to the complex mass, shape, dynamics, hydration and ionic shell, thus it is not possible to assign a specific mechanism to the different D value.

Both the Q25L and R41Q mutations have been reported in tumors sequenced on COSMIC [6]. The R41Q H-Ras mutation has been observed in multiple adenocarcinomas of the stomach, while the Q25L H-Ras mutation has been reported in one melanoma [5]. Our working hypothesis predicts that the increased binding affinity we observed for these two mutants will proportionally increase net PIP<sub>3</sub> production by PI3K. For example, it is predicted that the R41Q Ras variant will recruit 6 times more PI3K to the plasma membrane, which would result in a six-fold increase in net PIP<sub>3</sub> production compared to native Ras. Other studies have indicated that even a modest increase in PI3K recruitment results in excessive PIP<sub>3</sub> production linked to oncogenesis, observed in the PI3K $\alpha$  mutant H1047R [23]. Thus, small unregulated increases in PIP<sub>3</sub> production can drive excessive growth and result in oncogenesis. Hence, hyperactivation of PIP<sub>3</sub> signaling, found in many cancers, is hypothesized as a mechanism by which the Q25L and R41Q Ras variants may contribute to oncogenesis. Further research is needed to test whether these mutations do indeed increase PI3K recruitment and PIP<sub>3</sub> production by the predicted factors (see Future Studies).

***Binding Affinity of Control Ras Mutations.*** Both D38E and Y40C mutants have been shown to qualitatively decrease binding affinity to PI3K $\gamma$ , which is confirmed by our analysis [16]. The K<sub>D</sub> reported for the D38E variant was 600  $\pm$  100  $\mu$ M, indicating that this mutant has around 100 times weaker binding affinity than standard Ras. This is an especially interesting result because the substitution from aspartate to glutamate is a chemically conservative mutation

that would be expected to have minimal effect on binding affinity. We hypothesize that extension of the side chain by one methylene group in glutamate produces enough steric rearrangement to disrupt a large network of salt bridges and hydrogen bonding across the Ras-RBD binding interface observed in the crystal structure of the Ras-PI3K complex [16], accounting for this substantial decrease in binding affinity. The Y40C variant also demonstrated significantly reduced binding affinity ( $K_D$  of  $200 \pm 40 \mu\text{M}$ ), but to a lesser extent than the D38E variant. The G13R variant carries a mutation at a site distal to the Ras-RBD interface that was not found to have significantly different binding affinity compared to standard Ras, but was found to retain increased levels of bound GTP as expected. This mutation is in one of the hotspot mutations implicated in disrupting intrinsic and GAP-mediated GTP hydrolysis that upregulates all Ras effector pathways, but does not appear impact the binding affinity to PI3K $\gamma$ .

***Future Directions.*** An important next step is to test whether the R41Q and Q25L Ras variants with increased binding affinity to the RBD of PI3K $\gamma$  in solution will exhibit the predicted effects on full length PI3K membrane recruitment and lipid kinase activation on a target membrane surface. Single-molecule TIRF experiments will be performed by other lab members to anchor Standard H-Ras and selected variants to a target membrane, and to compare their abilities to recruit full length PI3K to the membrane and increase net PIP<sub>3</sub> production. We hypothesize that there will be an increase in net PIP<sub>3</sub> production proportional to the increase in binding affinity observed for these mutants (illustrated in Figure 8 for Q25L).

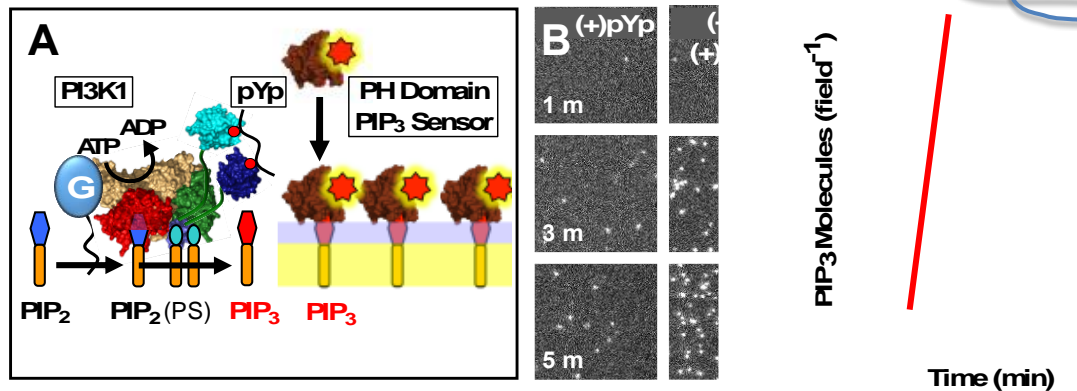


**Figure 8. Single molecule TIRF studies show maximal PIP<sub>3</sub> production in the presence of both Ras and phospho-tyrosine polypeptide.** (A) Schematic depiction of the single molecule PI3K activity assay. (B) Representative single molecule data. (C) Single molecule time courses. The Q25L and R41Q Ras variants are hypothesized to increase PI3K $\gamma$  recruitment and PIP<sub>3</sub> production, as would be revealed by an increased rate of PIP<sub>3</sub> production per minute (illustrated by red line for 3x activation by Q25L; R41Q would be expected to have an additional 2x greater rate of PIP<sub>3</sub> production than this red line indicates). Modified from Buckles et al (2017) [14], used with permission. Figure by Tom Buckles and Joe Falke.

Another important consideration is that Ras mutations show changes in binding affinity that is specific to a particular Ras effector. For example, while the Y40C variant has been shown to decrease binding affinity to full length PI3K $\gamma$ , it has demonstrated increased binding affinity to the PI3K $\alpha$  isoform [16]. The T35S and D38E Ras variants selectively activate the Raf signaling pathway, but show decreased binding affinity to PI3K $\alpha$ , PI3K $\delta$ , and PI3K $\gamma$  [16]. Effector-specific changes in binding affinity for Ras variants can be further explored by creating soluble constructs for the RBD of Raf, PI3K $\alpha$ , and PI3K $\delta$  for future use in microscale thermophoresis assays.

## References

- [1] Simanshu DK, Nissley DV, McCormick F. RAS Proteins and Their Regulators in Human Disease. *Cell*. 2017 Jun 29; 170(1):17-33.
- [2] Fernández-Medarde A, Santos E. Ras in cancer and developmental diseases. *Genes Cancer*. 2011 Mar; 2(3):344-58.
- [3] Karnoub AE, Weinberg RA. Ras oncogenes: split personalities. *Nat Rev Mol Cell Biol*. 2008 Jul; 9(7):517-31.
- [4] Fleming IR, Hannan JP, Swisher GH, Tesdahl CD, Martyr JG, Cordaro NJ, Erbse AH, Falke JJ. Binding of active Ras and its mutants to the Ras binding domain of PI-3-kinase: A quantitative approach to  $K_D$  measurements. *Anal Biochem*. 2023 Feb; 663:115019.
- [5] Schubbert S, Shannon K, Bollag G. Hyperactive Ras in developmental disorders and cancer. *Nat Rev Cancer*. 2007 Apr;7(4):295-308. doi: 10.1038/nrc2109. Erratum in: *Nat Rev Cancer*. 2007 Jul; 7(7):563.
- [6] Tate JG, Bamford S, Jubb HC, Sondka Z, Beare DM, Bindal N, Boutselakis H, Cole CG, Creatore C, Dawson E, Fish P, Harsha B, Hathaway C, Jupe SC, Kok CY, Noble K, Ponting L, Ramshaw CC, Rye CE, Speedy HE, Stefancsik R, Thompson SL, Wang S, Ward S, Campbell PJ, Forbes SA. COSMIC: the Catalogue Of Somatic Mutations In Cancer. *Nucleic Acids Res*. 2019 Jan; 47(D1):D941-D947.
- [7] Macaluso M, Russo G, Cinti C, Bazan V, Gebbia N, Russo A. Ras family genes: an interesting link between cell cycle and cancer. *J Cell Physiol*. 2002 Aug; 192(2):125-30.
- [8] Castellano E, Santos E. Functional specificity of ras isoforms: so similar but so different. *Genes Cancer*. 2011 Mar; 2(3):216-31.
- [9] Hobbs GA, Der CJ, Rossman KL. RAS isoforms and mutations in cancer at a glance. *J Cell Sci*. 2016 Apr; 129(7):1287-92.
- [10] Rauen KA. The RASopathies. *Annu Rev Genomics Hum Genet*. 2013; 14:355-69.
- [11] Gordon MT, Ziemba BP, Falke JJ. Single-molecule studies reveal regulatory interactions between master kinases PDK1, AKT1, and PKC. *Biophys J*. 2021 Dec 21; 120(24):5657-5673.

- [12] Samuels Y, Waldman T. Oncogenic mutations of PIK3CA in human cancers. *Curr Top Microbiol Immunol.* 2010; 347:21-41.
- [13] Ziemba BP, Falke JJ. A PKC-MARCKS-PI3K regulatory module links Ca<sup>2+</sup> and PIP<sub>3</sub> signals at the leading edge of polarized macrophages. *PLoS One.* 2018 May; 13(5).
- [14] Buckles TC, Ziemba BP, Masson GR, Williams RL, Falke JJ. Single-Molecule Study Reveals How Receptor and Ras Synergistically Activate PI3K $\alpha$  and PIP<sub>3</sub> Signaling. *Biophys J.* 2017 Dec 5; 113(11):2396-2405.
- [15] Gureasko J, Galush WJ, Boykevisch S, Sondermann H, Bar-Sagi D, Groves JT, Kuriyan J. Membrane-dependent signal integration by the Ras activator Son of sevenless. *Nat Struct Mol Biol.* 2008 May; 15(5):452-61.
- [16] Pacold ME, Suire S, Perisic O, Lara-Gonzalez S, Davis CT, Walker EH, Hawkins PT, Stephens L, Eccleston JF, Williams RL. Crystal structure and functional analysis of Ras binding to its effector phosphoinositide 3-kinase gamma. *Cell.* 2000 Dec 8; 103(6):931-43.
- [17] Martinez NG, Thieker DF, Carey LM, Rasquinha JA, Kistler SK, Kuhlman BA, Campbell SL. Biophysical and Structural Characterization of Novel RAS-Binding Domains (RBDs) of PI3K $\alpha$  and PI3K $\gamma$ . *J Mol Biol.* 2021 Apr 16; 433(8):166838.
- [18] Swisher GH, Hannan JP, Cordaro NJ, Erbse AH, Falke JJ. Ras-guanine nucleotide complexes: A UV spectral deconvolution method to analyze protein concentration, nucleotide stoichiometry, and purity. *Anal Biochem.* 2021 Apr 1; 618:114066.
- [19] Hannan JP, Swisher GH, Martyr JG, Cordaro NJ, Erbse AH, Falke JJ. HPLC method to resolve, identify and quantify guanine nucleotides bound to recombinant ras GTPase. *Anal Biochem.* 2021 Oct 15; 631:114338.
- [20] Jerabek-Willemsen M, Wienken CJ, Braun D, Baaske P, Duhr S. Molecular interaction studies using microscale thermophoresis. *Assay Drug Dev Technol.* 2011 Aug; 9(4):342-53.
- [21] Shaner NC, Lambert GG, Chammas A, Ni Y, Cranfill PJ, Baird MA, Sell BR, Allen JR, Day RN, Israelsson M, Davidson MW, Wang J. A bright monomeric green fluorescent

- protein derived from *Branchiostoma lanceolatum*. *Nat Methods*. 2013 May; 10(5):407-9
- [22] Killoran RC, Smith MJ. Conformational resolution of nucleotide cycling and effector interactions for multiple small GTPases determined in parallel. *J Biol Chem*. 2019 Jun; 294(25):9937-9948.
- [23] Wilkins MR, Gasteiger E, Bairoch A, Sanchez JC, Williams KL, Appel RD, Hochstrasser DF. Protein identification and analysis tools in the ExPASy server. *Methods Mol Biol*. 1999; 112:531-52.
- [24] Rubio I, Wittig U, Meyer C, Heinze R, Kadereit D, Waldmann H, Downward J, Wetzker R. Farnesylation of Ras is important for the interaction with phosphoinositide 3-kinase gamma. *Eur J Biochem*. 1999 Nov; 266(1):70-82.

## Appendices

*A.1: Methodology for HPLC Analysis, performed by Dr. Jonathan Hannon*

### ***HPLC analysis of the nucleotide mixture bound to Ras, and quantification of fractional Ras***

***activation.*** The mixture of guanine nucleotides (GXP) bound to each H-Ras protein prep was quantified via our HPLC protocol that has been previously validated and described in detail [28]. Briefly, following nucleotide loading, standard or variant GXP:H-Ras complexes were thawed on ice then washed 5 times in Wash Buffer (25 mM Hepes, pH 7.4, 140 mM KCl, 15 mM NaCl) to remove any remaining unbound nucleotides via centrifugation in spin dialysis concentrators (Vivaspin 500 with 10 kDa MW cutoff membrane (Sartorius)). After washing, the bound nucleotides were isolated from each H-Ras sample using a heat-extraction procedure in which the GXP:H-Ras complex was heated at 95 °C for 6 min using a MiniAmp thermocycler (Applied Biosystems) to denature the protein and release its bound nucleotide [28]. Samples were then chilled on ice for 2 min and precipitated protein was then removed by centrifugation resulting in a clarified solution of nucleotides derived from standard or variant H-Ras. HPLC-UV was used to determine the nucleotide composition of each clarified solution using an Agilent Technology 1260/1290 Infinity HPLC system in conjunction with a Phenomenex Gemini C18 reverse-phase analytical column fitted with a Phenomenex Standard Guard Cartridge System [28]. Mobile Phase conditions were 92.5 mM potassium phosphate (KH<sub>2</sub>PO<sub>4</sub>), 9.25 mM tetrabutylammonium bromide, pH to 6.4 with 7.5% acetonitrile. All samples were run in the mobile phase at a flow rate of 1.3 ml/min for 9 min at 22 °C. A mixture of standard nucleotides heated to 95 °C for 6 min was injected to test proper HPLC system operation and confirm the characteristic retention times for each nucleotide in the UV absorbance trace. Next, following extraction from a standard or variant H-Ras protein, each clarified GXP nucleotide mixture was injected, and the identities

of the individual nucleotide components were determined from the characteristic retention times of their UV peaks. For each H-Ras protein prep, triplicate (or more) HPLC analyses were carried out on extracted GXP nucleotide mixtures from three separate protein samples. Our previously published HPLC protocol detailed the identities and origins of the resulting nucleotide peaks, including the effects of heat extraction on each nucleotide as required to relate each HPLC peak to its parent nucleotide in the Ras protein population [28]. Briefly, as illustrated in Fig. 5 and Table S1 for representative H-Ras preps, two major peaks were observed for proteins loaded with GMPPNP: (i) The  $\Delta$ GMPPNP (or GMPPN) component represents the GMPPN molecules extracted from the GMPPNP-activated H-Ras subpopulation, owing to the virtually complete, intentional hydrolysis of GMPPNP to GMPPN during the heat extraction step. (ii) The GDP component represents the GDP molecules extracted from the GDP-inactivated H-Ras subpopulation, which originated from intracellular nucleotide loading of H-Ras and remained bound during protein purification and nucleotide exchange. Up to three other minor peaks were sometimes observed for proteins loaded with GMPPNP: (i) low but detectable levels of GMP were observed when heat extraction yielded minor hydrolysis of GDP, (ii) low but detectable levels of GMPPNP were observed when its hydrolysis to GMPPN during heat extraction was not fully achieved, and (iii) GTP was sometimes observed at low levels for standard H-Ras, or at moderate levels for H-Ras mutants with defective GTP hydrolysis. For proteins loaded with GDP, the sole major peak observed was GDP, and only minor peaks were sometimes observed for GMP and GTP. The individual extracted nucleotides observed for a given H-Ras sample were quantified by integration of their HPLC peaks as previously described [28] and their relative peak areas were used to calculate the fractional activation of the starting H-Ras population as follows. The H-Ras subpopulation in the

active state was defined by the sum of the activating nucleotides ( $\Delta$ GMPPNP (+) GMPPNP (+) GTP). The H-Ras subpopulation in the inactive state was defined by the sum of the GDP-derived, inactivating nucleotides (GDP (+) GMP). Together these yielded the fraction of the total H-Ras population in active state, calculated as the ratio of the activating nucleotides ( $\Delta$ GMPPNP (+) GMPPNP (+) GTP) to the total nucleotides ( $\Delta$ GMPPNP (+) GMPPNP (+) GTP) (+) GDP (+) GMP) [28]. Notably, the fractional activation of the H-Ras population was observed to vary from 49% to 84% between different H-Ras preps, due largely to variation in the efficiency of the GMPPNP loading step. This variation emphasized the importance of HPLC quantitation of each protein prep to enable accurate and reproducible titrations with active H-Ras in MST binding studies. Without such HPLC quantitation, up to 2-fold uncertainty could exist in active H-Ras KD measurements.

A.2: Table S1. HPLC loadings of each Ras purification used in MST assays

| <b>Protein<br/>(Nx3)</b>                | <b>GMP<br/>(% ± SD)</b> | <b>ΔGMPPNP<br/>(% ± SD)</b> | <b>GDP<br/>(% ± SD)</b> | <b>GMPPNP<br/>(% ± SD)</b> | <b>GTP<br/>(% ± SD)</b> | <b>Active<br/>(% ± SD)</b> | <b>Inactive<br/>(% ± SD)</b> |
|---|-------------------------|-----------------------------|-------------------------|----------------------------|-------------------------|----------------------------|------------------------------|
| <b>Standard Ras<br/>(N=3x3)</b>         | 1.7 ± 0.7               | 50.2 ± 0.4                  | 43.8 ± 0.3              | 1.3 ± 0.3                  | 2.9 ± 0.2               | 54.4 ± 0.9                 | 45.6 ± 1                     |
|   | 2.1 ± 0.2               | 60.5 ± 1.0                  | 35.6 ± 0.1              | ND                         | 1.8 ± 1.0               | 62.3 ± 1.9                 | 37.7 ± 0.2                   |
|   | 2.2 ± 0.3               | 54.4 ± 0.5                  | 40.6 ± 0.3              | 1.4 ± 0.5                  | 1.4 ± 0.7               | 57.2 ± 1.8                 | 42.8 ± 0.6                   |
| <b>G13R<br/>(N=2x3)</b>                 | 2.6 ± 1.3               | 76.7 ± 0.8                  | 13.6 ± 0.4              | 2.4 ± 0.9                  | 4.6 ± 0.3               | 83.7 ± 2                   | 16.3 ± 1.8                   |
|   | 1.4 ± 0.5               | 60.3 ± 0.2                  | 23.2 ± 0.5              | 2.3 ± 0.3                  | 12.8 ± 0.4              | 75.4 ± 0.9                 | 24.6 ± 1                     |
| <b>Q25L<br/>(N=5x3)</b>                 | 3.5 ± 0.3               | 71.1 ± 0.7                  | 23.8 ± 0.7              | 1.0 ± 0.5                  | 0.7 ± 0.6               | 72.8 ± 1.9                 | 27.2 ± 1                     |
|   | 1.6 ± 0.0               | 57.4 ± 0.6                  | 38.0 ± 0.9              | 1.6 ± 0.5                  | 1.5 ± 0.1               | 60.5 ± 1.2                 | 39.5 ± 1                     |
|   | 2.0 ± 0.5               | 49.0 ± 0.2                  | 44.3 ± 0.5              | 2.2 ± 0.1                  | 2.5 ± 0.1               | 53.7 ± 0.5                 | 46.3 ± 1                     |
|   | 1.7 ± 0.4               | 60.7 ± 0.8                  | 37.2 ± 0.3              | 0.4 ± 0.6                  | ND                      | 61.1 ± 1.4                 | 38.9 ± 0.7                   |
|   | 1.9 ± 0.4               | 48.9 ± 0.5                  | 47.9 ± 1.2              | 1.1 ± 1                    | 0.2 ± 0.2               | 50.2 ± 1.6                 | 49.8 ± 1.6                   |
| <b>D38E<br/>(N=2x3)</b>                 | 2.2 ± 0.4               | 51.8 ± 0.7                  | 43.1 ± 0.2              | 1.7 ± 0.2                  | 1.2 ± 0.7               | 54.7 ± 1.5                 | 45.3 ± 0.6                   |
|   | 2.6 ± 0.4               | 48.3 ± 0.3                  | 48.2 ± 0.4              | 0.9 ± 0.6                  | ND                      | 49.2 ± 0.8                 | 50.8 ± 0.8                   |
| <b>Y40C<br/>(N=2x3)</b>                 | 2.1 ± 0.4               | 55.1 ± 0.8                  | 40.9 ± 0.3              | ND                         | 1.9 ± 0.7               | 57.0 ± 1.5                 | 43.0 ± 0.7                   |
|   | 2.0 ± 0.3               | 58.9 ± 0.3                  | 36.2 ± 0.3              | 0.7 ± 0.2                  | 2.2 ± 0.1               | 61.8 ± 0.5                 | 38.2 ± 0.6                   |
| <b>R41Q<br/>(N=3x3)</b>                 | 1.7 ± 0.2               | 78.2 ± 0.1                  | 17.5 ± 0.3              | 1.5 ± 0.1                  | 0.9 ± 0.3               | 80.6 ± 0.5                 | 19.4 ± 0.5                   |
|   | 1.0 ± 0.2               | 85.8 ± 0.3                  | 10.5 ± 0.3              | 2.1 ± 0.1                  | 0.7 ± 0.2               | 88.6 ± 0.6                 | 11.4 ± 0.5                   |
|   | ND                      | 66.8 ± 0.2                  | 30.3 ± 0.4              | 2.3 ± 0.1                  | 0.2 ± 0.1               | 69.3 ± 0.4                 | 30.7 ± 0.4                   |
| <b>Standard Ras<br/>GDP<br/>(N=3x3)</b> | 3.0 ± 0.5               | ND                          | 94.6 ± 0.6              | ND                         | 2.4 ± 0.1               | 2.4 ± 0.1                  | 97.6 ± 1.1                   |
|   | 2.7 ± 0.5               | ND                          | 97.1 ± 0.8              | ND                         | 0.2 ± 0.3               | 0.2 ± 0.3                  | 99.8 ± 1.2                   |
|   | 3.2 ± 0.5               | ND                          | 95.0 ± 0.6              | ND                         | 1.8 ± 0.6               | 1.8 ± 0.6                  | 98.2 ± 1.1                   |

**Table S1 Summary.** HPLC Quantification of Bound Nucleotides and Fractional Activation for Individual Preparations of Ras Variants Shown are the relative mole percentages of the indicated bound nucleotides for each individual Ras preparation utilized in this study (data of Figures 5, 6 and Table 1 in main text). ND = Not Detected. The fractional activation of a specific Ras prep is defined as the sum of the mole percentages of the nucleotides derived from activating GMPPNP and GTP (or, ΔGMPPNP (+) GMPPNP (+) GTP). The data in Table S1 was collected by Dr. Jonathan Hannon and Shea O’Conner, compiled by Corey Tesdahl. From Fleming et al (2022), used with permission.